Proceedings of the Korean Nuclear Society Autumn Meeting
Taejon, Korea, October 2000

Pre-Analysis of Liquid Metal Natural Circulation Experiment

Chan-Soo Kim, Ho S. Chu, Sang H. Yoon, Seung D. Lee, Kune Y. Suh

Department of Nuclear Engineering, Seoul National University
San 56-1 Shinrim-dong, Kwanak-gu, Seoul, 151-742, Korea
Phone : +82-2-880-8281, Fax : +82-2-883-0827, Email : chan2117@snu.ac.kr

Abstract

In this study, the pre-analysis is performed for the liquid metal natural circulation experiment. The natural circulation is the advantage of a liquid metal reactor as the reactor safety. We will use the low melting eutetic metal alloy instead of the lead-bismuth coolant of a liquid metal reactor to prove the natural circulation potential of liquid metal. In the pre-analysis, the first principle calculation and CFX 4.2 code were used. In the large pipe diameter, the natural circulation experiment can be performed widely and safely. Therefore, we determine that the pipe diameter in the test loop is 10 cm.

1. Introduction

A liquid metal reactor (LMR), named PEACER (Proliferation-resistant, Environmental-friendly, Accident-tolerant, Continuable-energy, Economical Reactor) is being designed at the Seoul National University with the metallic U-Pu-Th fuel and the lead-bismuth (Pb-Bi) coolant[1]. PEACER consists of the primary liquid loop and the steam producing secondary loop. First-principle calculations were performed to analyze the natural circulation heat removal from the core of an LMR. The Pb-Bi coolant has low chemical activities with air or water. The steam generating system can directly be coupled to primary liquid metal system without intermediate heat exchangers.

In fast reactors, the decay heat is generally removed by the forced convection of the coolant by the pumps. If the pumps are tripped, buoyancy driven flows play an important role. Natural circulation can provide the mechanism for transferring heat away from the core region up to the cooler parts of the primary loop. So, the natural circulation potential is a key characteristic of the LMR design. Under natural circulation conditions, the liquid metal flow is driven by buoyancy. The elevation between the thermal centers of the core and the steam generators corresponds to the buoyancy pressure head. The

decay heat fraction that can be removed by the natural circulation due to the distance between thermal centers and the temperatures difference was determined. The elevation difference of 4.5m between the thermal centers of the core and the steam generator was shown to remove as much as 10% of the thermal reactor power. Note that the decay heat level is below 10% at shutdown.

The natural circulation heat removal capability of the liquid metal is to be evaluated in this experiment. We will use the low temperature (70℃) melting eutectic metal alloy instead of Pb-Bi in a scaled down test loop. Table 1 compares the material properties of Pb-Bi [2] and the low temperature melting eutectic metal alloy[3].

2. Model Description

2.1 First Principle Calculation

As pre-analysis for the experiment we calculated the required input power to the heating section given the velocity of the eutectic metal alloy flow in pipes with four different diameters. In this analysis, the calculation condition is one-dimensional, steady-state, single-phase flow[4]. Results from the analysis are obtained as functions of the Re number, heat flux on the surface of heating section, the power of the heater, the temperature difference between the hot and cold regions with four different pipe diameters, respectively. Figure 1 presents the noding scheme diagram for the pre-analysis. The nodes were divided into the inlet and outlet of the heating section, cooling section, four elbows and the piping.

The pressure difference between the nodes consists of the friction between the wall and the fluid, the acceleration, and the form loss as:

$$\Delta p_{i,j} = \Delta p_f + \Delta p_g + \Delta p_a + \Delta p_{form} \tag{1}$$

In more detail, the pressure differences between the two nodes are determined as:

$$p_1 = p_2 + f\frac{|h_2 - h_1|}{D}\frac{G^2}{r_1 + r_2} + \frac{r_1 + r_2}{2}g(h_2 - h_1) + \frac{G^2}{2}\left(\frac{1}{r_2} - \frac{1}{r_1}\right) \tag{2}$$

$$p_2 = p_3 + f\frac{|h_3 - h_2|}{D}\frac{G^2}{r_2 + r_3} + \frac{r_2 + r_3}{2}g(h_3 - h_2) + \frac{G^2}{2}\left(\frac{1}{r_3} - \frac{1}{r_2}\right) \tag{3}$$

$$p_3 = p_4 + \frac{r_3 + r_4}{2}g(h_4 - h_3) + \frac{G^2}{2}\left(\frac{1}{r_4} - \frac{1}{r_3}\right) + K_{elbow}\frac{G^2}{r_3 + r_4} \tag{4}$$

$$p_4 = p_5 + f\frac{L}{D}\frac{G^2}{r_4 + r_5} + \frac{G^2}{2}\left(\frac{1}{r_4} - \frac{1}{r_5}\right) \tag{5}$$

$$p_5 = p_6 + \frac{r_5 + r_6}{2}g(h_6 - h_5) + \frac{G^2}{2}\left(\frac{1}{r_6} - \frac{1}{r_5}\right) + K_{elbow}\frac{G^2}{r_6 + r_5} \tag{6}$$

$$p_6 = p_7 + f\frac{|h_7 - h_6|}{D}\frac{G^2}{r_6 + r_7} + \frac{r_6 + r_7}{2}g(h_7 - h_6) + \frac{G^2}{2}\left(\frac{1}{r_7} - \frac{1}{r_6}\right) \tag{7}$$

$$p_7 = p_8 + f\frac{|h_8 - h_7|}{D}\frac{G^2}{r_7 + r_8} + \frac{r_7 + r_8}{2}g(h_8 - h_7) + \frac{G^2}{2}\left(\frac{1}{r_8} - \frac{1}{r_7}\right) \tag{8}$$

$$p_8 = p_9 + f\frac{|h_9 - h_8|}{D}\frac{G^2}{r_8 + r_9} + \frac{r_8 + r_9}{2}g(h_9 - h_8) + \frac{G^2}{2}\left(\frac{1}{r_9} - \frac{1}{r_8}\right) \tag{9}$$

$$p_9 = p_{10} + \frac{r_9 + r_{10}}{2}g(h_{10} - h_9) + \frac{G^2}{2}\left(\frac{1}{r_{10}} - \frac{1}{r_9}\right) + K_{elbow}\frac{G^2}{r_9 + r_{10}} \tag{10}$$

$$p_{10} = p_{11} + f\frac{L}{D}\frac{G^2}{r_{10} + r_{11}} + \frac{G^2}{2}\left(\frac{1}{r_{11}} - \frac{1}{r_{10}}\right) \tag{11}$$

$$p_{11} = p_{12} + \frac{r_{11} + r_{12}}{2}g(h_{12} - h_{11}) + \frac{G^2}{2}\left(\frac{1}{r_{11}} - \frac{1}{r_{12}}\right) + K_{elbow}\frac{G^2}{r_{11} + r_{12}} \tag{12}$$

$$p_{12} = p_1 + f\frac{|h_1 - h_{12}|}{D}\frac{G^2}{r_1 + r_{12}} + \frac{r_1 + r_{12}}{2}g(h_1 - h_{12}) + \frac{G^2}{2}\left(\frac{1}{r_1} - \frac{1}{r_{12}}\right) \tag{13}$$

The density in each node is defined as:

$$\begin{aligned} r_i &= r_c \quad for\ i = 1,8 \sim 12 \\ r_i &= r_h \quad for\ i = 2 \sim 7 \end{aligned} \tag{14}$$

Utilizing the density in equation (14), the summation of equations (2) to (13) yields the following equation:

$$\begin{aligned} &f\frac{L}{D}\left(\frac{G^2}{2r_c} + \frac{G^2}{2r_h}\right) + f\frac{G^2}{2r_h}\left\{\frac{|h_3 - h_2|}{D} + \frac{|h_7 - h_6|}{D}\right\} + f\frac{G^2}{2r_c}\left\{\frac{|h_9 - h_8|}{D} + \frac{|h_1 - h_{12}|}{D}\right\} \\ &+ f\frac{G^2}{r_h + r_c}\left\{\frac{|h_2 - h_1|}{D} + \frac{|h_8 - h_7|}{D}\right\} + K_{elbow}\left(\frac{G^2}{r_h} + \frac{G^2}{r_c}\right) = (r_c - r_h)g\frac{h_7 + h_8 - h_1 - h_2}{2} \end{aligned} \tag{15}$$

Equation (15) is the governing equation for the natural circulation. It demonstrates that under natural circulation condition, the flow is driven entirely by the balance between the buoyancy-

generated pressure head and the pressure drop from friction and form loss. If there is no difference in density between the hot leg and the cold leg, equation (15) may be simplified as:

$$f\frac{|h_6-h_9|+L}{D}+2K_{elbow}\frac{G^2}{r_c}=(r_c-r_h)g\frac{h_7+h_8-h_2-h_1}{2} \quad (16)$$

The density dependence on temperature can be assumed to vary linearly pursuant to the Boussinesq approximation. The difference is thus defined as:

$$r_c-r_h=r_c b\Delta T \quad (17)$$

The difference in temperature between the hot leg and the cold leg consists of the mass flux, pipe diameter, heater power, heat flux and heated area as

$$G\frac{pD^2}{4}c_p\Delta T=Q=q''pD(h_2-h_1) \quad (18)$$

The material properties of the eutectic metal alloy used in this study are summarized in Table 1. The friction factor is defined as follows, while K_{elbow} [5] is summarized in Table 2.

$$\begin{array}{ll} f=64/\mathrm{Re}_D & for \quad \mathrm{Re}_D\le 2300 \\ 0.184\,\mathrm{Re}_D^{-0.2} & for \quad \mathrm{Re}_D>2300 \end{array} \quad (19)$$

2.2 Code Analysis Using CFX 4.2

Pre-analysis was also conducted for the liquid metal natural circulation using CFX4.2, which is a three-dimensional thermal-hydraulic analysis code. Results of the code analysis were compared with those of the first principle calculation wit a view to appreciating the natural circulation capability of the selected low temperature melting metal. Figure 2 shows the three-dimensional, cylindrical model to compute the distribution of flow temperature, pressure, velocity, etc. The liquid metal circulates through the cylindrical pipe driven by the temperature difference between the heat source and the heat sink. In the modeling, the heat flux of the heat source is 28 kW/m^2.

3. Results and Discussion

3.1 First Principle Calculation

Figures 3 to 7 illustrate results from equations (16), (17) and (18). Figure 3 presents the Re number given the velocity for different pipe diameters. As the diameter of the pipe gets larger, the minimum

velocity of the region of turbulence decreases. The diameter of the pipe must be large for the natural circulation flow to be turbulent.

Figure 4 shows the density difference with differing pipe diameters. The maximum density difference is 0.0025 kg/m^3. Density of the eutectic metal alloy is large enough to assume that the density in the cold leg is equal to the density in the hot leg. In addition, the small diameter of the pipe renders the difference in density between the hot leg and the cold leg large given the flow velocity.

Figure 5 shows the temperature difference between the hot leg and the cold leg. The smaller pipe produces larger temperature difference given the flow velocity. This is because the smaller pipe decreases the mass flow rate given the flow velocity. The result is consistent with that in Figure 3. Because the low temperature melting eutectic metal alloy used in this experiment is burnable over 150°C, the diameter of the pipe must be large enough to cover the wide velocity range of this experiment.

Figure 6 shows the average heat flux of the heated section with different diameters. The larger the pipe diameter, the larger the heat flux. Therefore, the temperature of the surface in the heated section may be higher than 150°C. Because the small pipe will tend to increase the temperature difference given the flow velocity as shown Figure 5, partial burning of the low temperature melting eutectic metal alloy must be allowed in the large pipe.

Figure 7 presents the heater power in the heated section. The heater power in the small pipe is smaller than that in the large pipe. This shows that the heat removal is more effective in the large pipe given the flow velocity.

We thus decided to adopt the pipe diameter of 10 cm based on the computed results. In this experiment, the maximum natural circulation velocity will be about 3.5 cm/s according to the pre-analysis.

3.2 Code Analysis Using CFX 4.2

Using the CFX 4.2 code, the analysis was performed under the same geometrical condition as in the experiment to be conducted. Especially, we assumed that the average heat flux of the heat source is 28 kW/m^2. The steady turbulent three-dimensional basic equations for buoyancy flow and heat transfer are solved using the SIMPLEC algorithm and the body-fitted grid at the rectangular coordinates [6], [7], [8].

Figure 8 (a) proves that the velocity of 2.2 cm/s approximately approaches the average inner

velocity, which is smaller than that of first principle calculation method including the elbow effect. But the velocity of CFX 4.2 is similar to that of first principle calculation method including the screwed elbow effect. The form loss by the elbow effect in CFX 4.2 is larger than that in the first principle calculation. In case of the elbow effect, the surface velocity at the inner wall is larger than the average velocity at the inner wall as shown in Fig. 8 (b).

Figure 9 (a) shows the temperature distribution at the outer surface. We know that the temperature is partially very high at the low-left heat source of the whole system. The temperature difference between the hot region and the cold region is about 7.4 K. This result is also similar to 7.0 K of the first principle calculation method with the elbow effect. The inner wall temperature increases because the velocity increases at the inner wall by the elbow effect. Figure 9 (b) shows the velocities profile at the whole inner system. Because the flow temperature of the lower heat source at the wall is high, the velocity at the wall is large as shown in Fig 9 (b). The flow distribution in the hot region becomes fully developed in the turbulent region as the liquid metal flows into the adiabatic pipes. But the flow temperature distribution in the cold region decreases at the wall and the liquid metal flow velocity at the wall decreases against the hot region

4. Conclusion

We performed a pre-analysis for a natural circulation heat transfer experiment with a low temperature melting metal coolant. Material properties of the coolant are similar to those for Pb-Bi, which has a good natural circulation capability. Under natural circulation conditions, the flow is driven by the buoyancy. The elevation between the thermal centers of the heat source and the heat sink corresponds to the buoyancy pressure head. The natural circulation can remove the generated heat. Both the first principle model and CFX 4.2 yielded the consistent conclusion that the elevation difference between the thermal centers is the governing parameter. The large pipe diameter makes the experiments be performed as the wide range. So, we determine that the pipe diameter in the test loop is 10 cm.

A one-dimensional flow loop model was developed to analyze the state of a natural circulation condition. Along the primary coolant path we solved the steady state momentum equation and energy equation at a one-dimensional lumped node. The flow loop shows the simple and explicit results of natural circulation heat removal. The low temperature melting metal coolant has a good natural circulation potential and only the condenser can remove the generated heat.

REFERENCES

1. J. E. Chang and K. Y. Suh, 2000, "Natural circulation heat transfer in a liquid metal reactor," Proceeding of the 8th International Conference on Nuclear Engineering, 8522, Baltimore, MA, USA, 2-6 April
2. Hwang et al, 1998, "A study on the physicochemical properties of nonreactive liquid metal," Final Report, KISTEP
3. Park et al, 1999, "Natural convection heat transfer with crust formation in the molten metal pool," Nuclear Technology, vol.127, pp 66-80
4. N.E. Todreas and M. S. Kazimi, 1990, "Nuclear system II," Hemisphere Publishing Corporation, New York, NY, USA
5. F. M. White, 1999, "Fluid Mechanics," 4th ed., McGraw-Hill International Editions, Singapore
6. U.K. AEA Technology, CFX 4.2: Pre-processing, Oxfordshire, United Kingdom, 1997a
7. U.K. AEA Technology, CFX 4.2: Solver, Oxfordshire, United Kingdom, 1997b
8. U.K. AEA Technology, CFX 4.2: Post-processing, Oxfordshire, United Kingdom, 1997c

Table 1. Comparison of material thermophysical properties

Properties	Pb-Bi	Low temperature melting metal
Melting point [℃]	125	70
Density [kg/m^3]	10240	9383.2
Volumetric thermal expansion coefficient [K^{-1}]	2.2×10^{-5}	2.2×10^{-5}
Thermal conductivity [W/mK]	11.9	18.9
Specific heat [J/kgK]	146.4	167.5
Kinematic viscosity [m^2/s]	1.5×10^{-5}	2×10^{-5}
Pr	0.019	0.013

Table 2 Resistance coefficients for 90º regular flanged elbows

Pipe diameter [cm]	2.5	5.0	10.0
Resistance coefficients	0.5	0.39	0.30

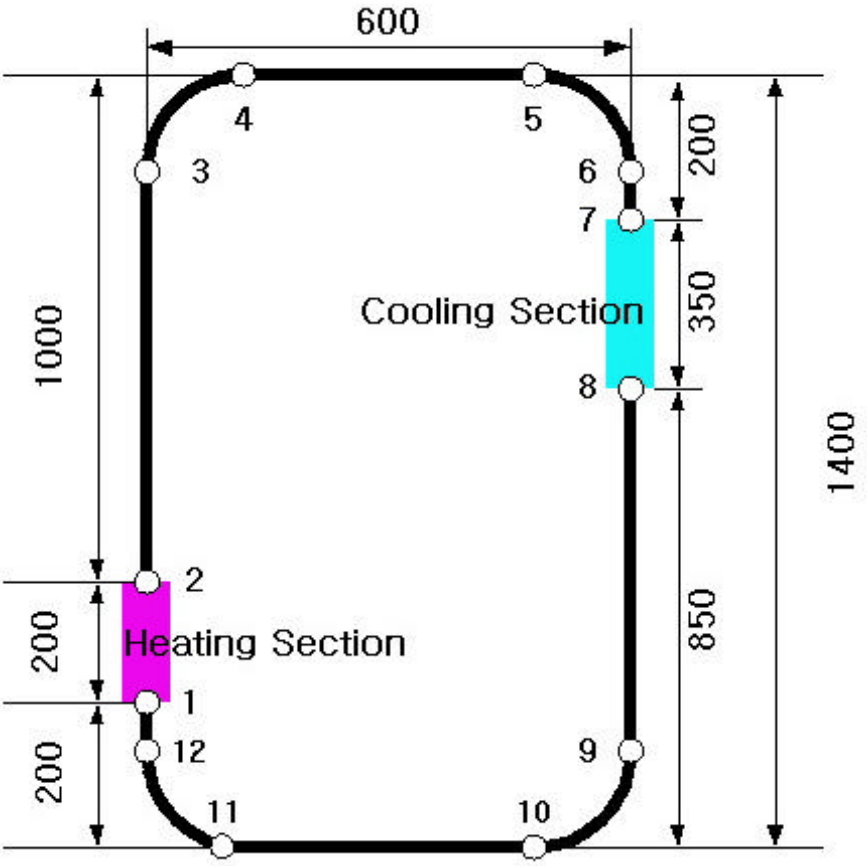

Fig. 1 Flow loop nodalization

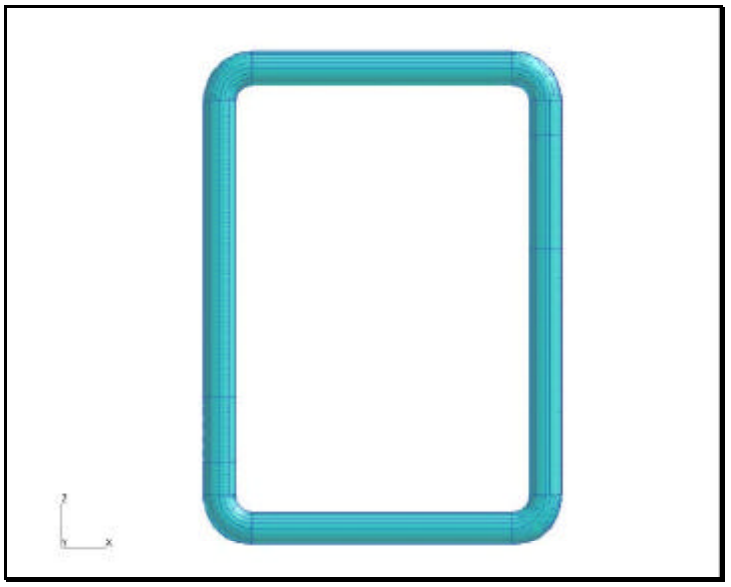

Fig. 2 CFX 4.2 analysis model

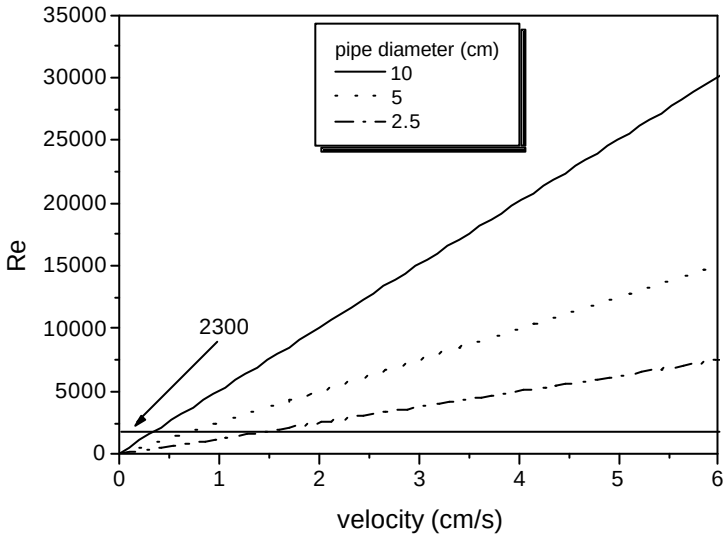

Fig. 3 Re variation given the flow velocity

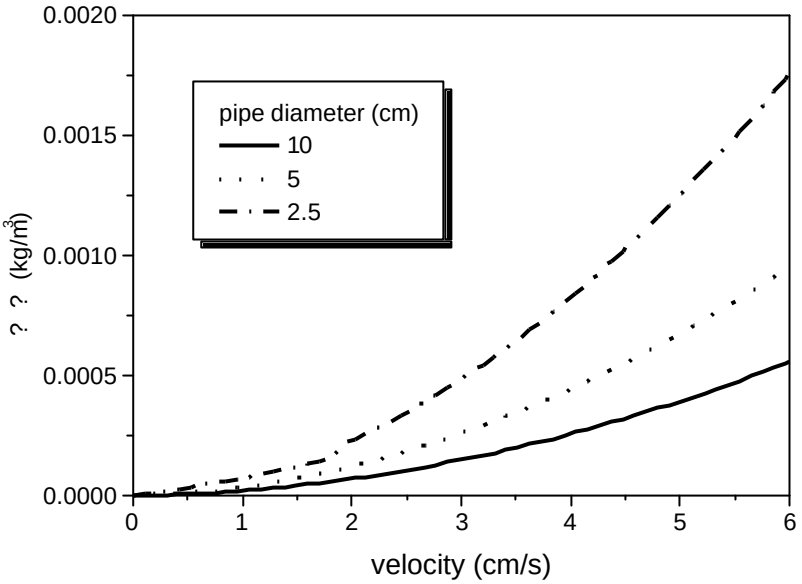

Fig. 4 Density difference variation given the flow velocity

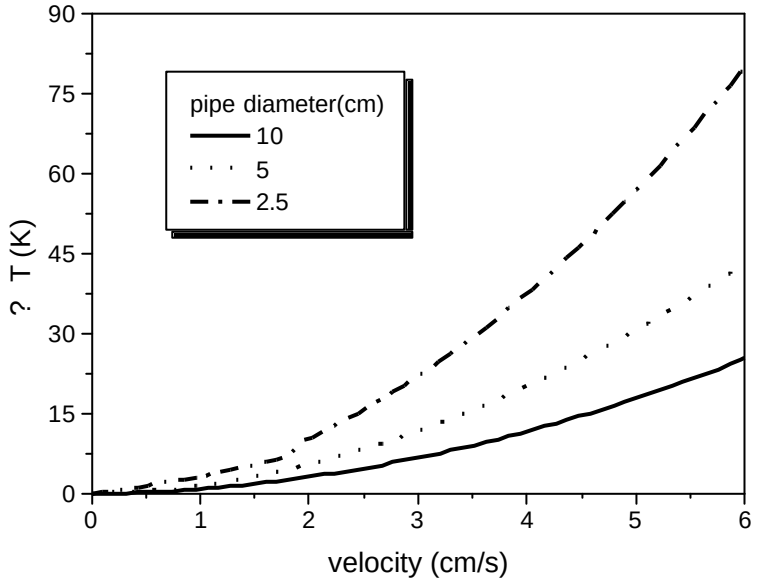

Fig. 5 Temperature difference variation given the flow velocity

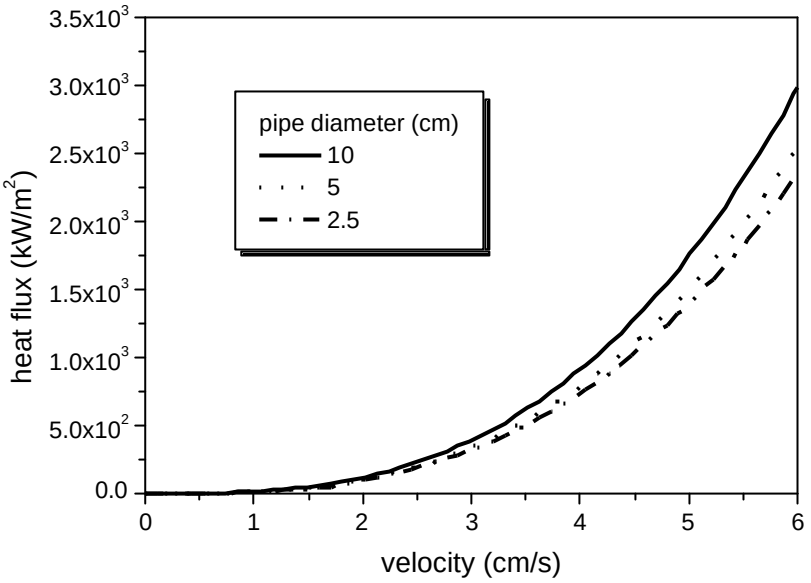

Fig. 6 Heat flux variation given the flow velocity

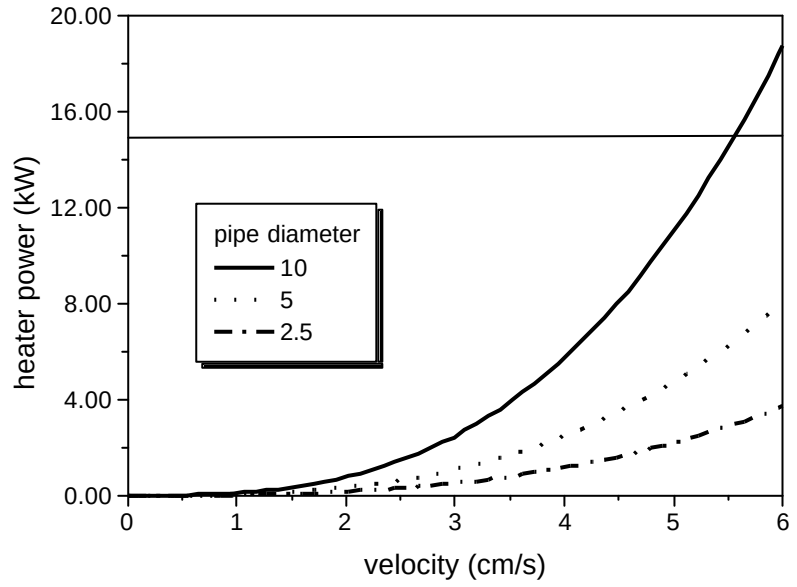

Fig. 7 Heater power variation given the flow velocity

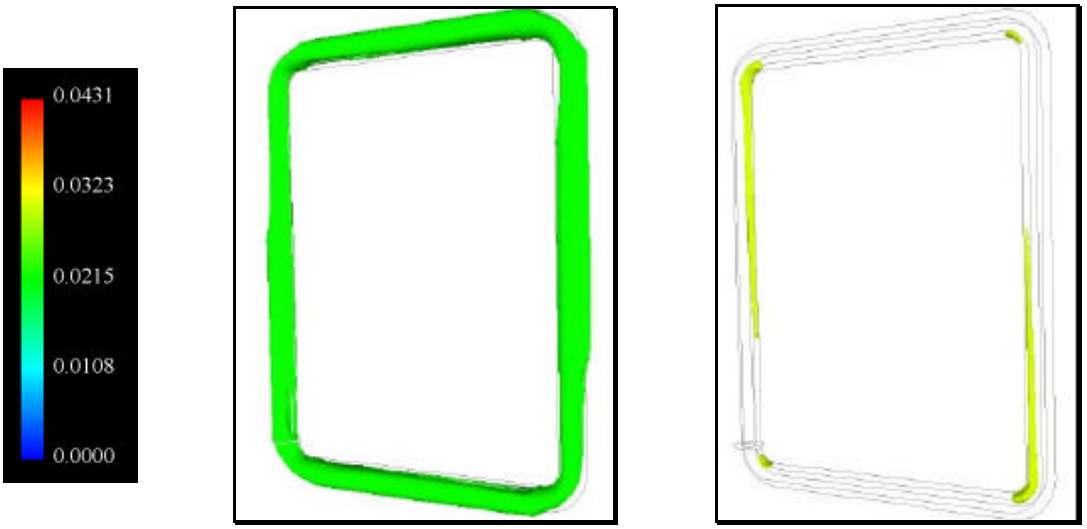

(a) 0.02 m/s (b) 0.031 m/s

Fig. 8 CFX 4.2 iso-velocity profile

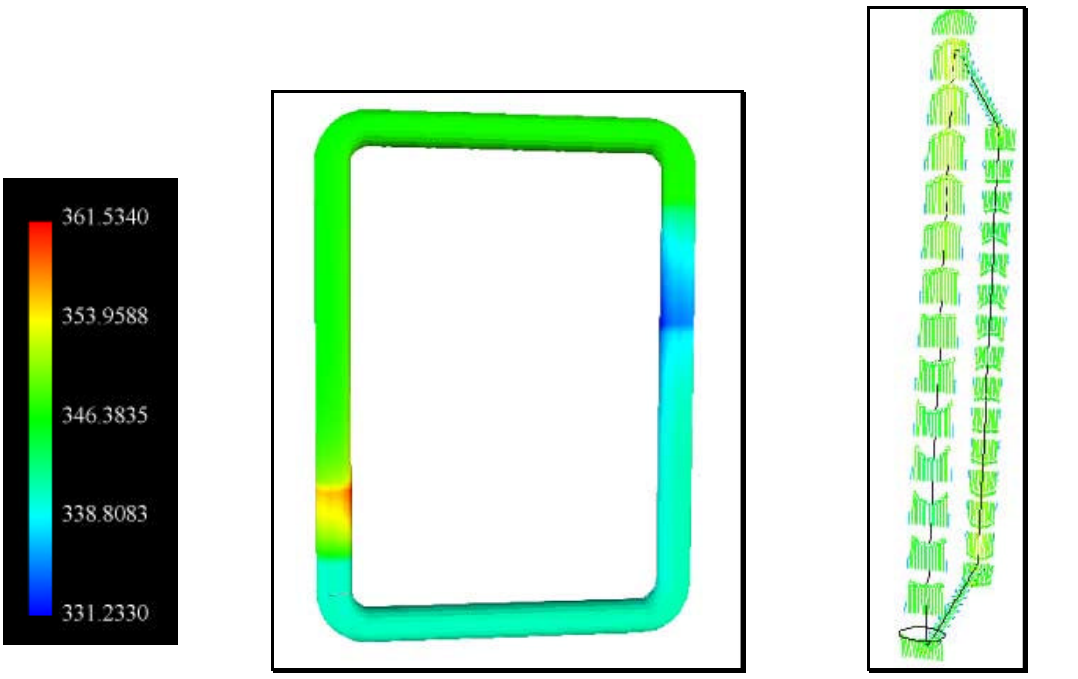

(a) Surface temperature [K] (b) Vector distribution

Fig. 9 CFX 4.2 surface temperature distribution and inner vector profile